ACS Catalysis

Research Article

pubs.acs.org/acscatalysis

Conversion of Dimethyl Ether to 2,2,3-Trimethylbutane over a Cu/BEA Catalyst: Role of Cu Sites in Hydrogen Incorporation

Joshua A. Schaidle,*[,†] Daniel A. Ruddy,[‡] Susan E. Habas,[†] Ming Pan,[†] Guanghui Zhang,[§] Jeffrey T. Miller,[§] and Jesse E. Hensley[†]

[†]National Bioenergy Center and [‡]Chemistry and Nanoscience Center, National Renewable Energy Laboratory, Golden, Colorado 80401, United States

[§]Chemical Sciences and Engineering Division, Argonne National Laboratory, Argonne, Illinois 60439, United States

Supporting Information

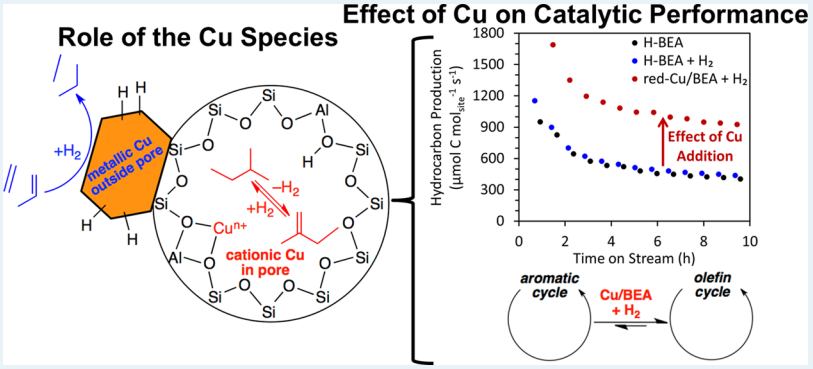

ABSTRACT: Recently, it has been demonstrated that methanol and/or dimethyl ether can be converted into branched alkanes at low temperatures and pressures over large-pore acidic zeolites such as H-BEA. This process achieves high selectivity to branched C_4 (e.g., isobutane) and C_7 (e.g., 2,2,3-trimethylbutane) hydrocarbons. However, the direct homologation of methanol or dimethyl ether into alkanes and water is hydrogen-deficient, resulting in the formation of unsaturated alkylated aromatic residues, which reduce yield and can contribute to catalyst deactivation. In this paper we describe a Cu-modified H-BEA catalyst that is able to incorporate hydrogen from gas-phase H_2 cofed with dimethyl ether into the desired branched alkane products while maintaining the high C_4 and C_7 carbon selectivity of the parent H-BEA. This hydrogen incorporation is achieved through the combination of metallic Cu nanoparticles present on the external surface of the zeolite, which perform H_2 activation and olefin hydrogenation, and Lewis acidic ion-exchanged cationic Cu present within the H-BEA pores, which promotes hydrogen transfer. With cofed H_2, this multifunctional catalyst achieved a 2-fold increase in hydrocarbon productivity in comparison to H-BEA and shifted selectivity toward products favored by the olefin catalytic cycle over the aromatic catalytic cycle.

KEYWORDS: *triptane, dimethyl ether, homologation, zeolite, H-BEA, Cu/H-BEA, olefin catalytic cycle, aromatic catalytic cycle, hydrogen incorporation*

1. INTRODUCTION

Zeolite materials, combining both Brønsted acidity and confinement effects, possess unique catalytic properties directly relevant to biomass-to-fuels conversion processes. Specifically, the C_1 chemistry of methanol conversion over acidic zeolites presents a promising route for the conversion of biomass-derived synthesis gas into a variety of hydrocarbons: light olefins, aromatics, branched alkanes, and gasoline-range hydrocarbons.[1−3] The types of hydrocarbons produced are controlled by the zeolite type and the operating conditions. Of particular interest is the recent work by Iglesia and co-workers demonstrating the selective synthesis of triptane (2,2,3-trimethylbutane) and isobutane by reacting dimethyl ether (DME) over large-pore acidic zeolites (e.g., H-BEA) at relatively low temperatures (180−220 °C) and pressures (60−250 kPa of DME).[4−7] The high selectivity to branched C_4 and C_7 paraffins and olefins is controlled by the relative rates of methylation-to-hydrogen transfer, carbocation stability, and facile β scission of C_{8+} chains.[4] Due to the hydrogen deficiency of DME homologation to alkane products, unsaturated residues are also formed (e.g., alkylated aromatics such as hexamethylbenzene (HMB)), which decrease the yield of the desired alkanes and can cause catalyst deactivation.[4,6] The stoichiometric reaction for DME homologation to form triptane and HMB is provided in eq 1.

$$33CH_3OCH_3 \rightarrow 6C_7H_{16} + 33H_2O + 2C_6(CH_3)_6[HMB] \quad (1)$$

Received: July 15, 2014
Revised: January 23, 2015
Published: February 19, 2015

DOI: 10.1021/cs501876w
ACS Catal. 2015, 5, 1794−1803

To address this hydrogen deficiency, Simonetti et al. demonstrated that alkanes cofed with DME could provide the required hydrogen when a hydride transfer cocatalyst, adamantane, was present.[6] However, the use of low-volatility adamantane in a gas-phase industrial process could create additional challenges. Therefore, we hypothesized that the incorporation of a metal into/onto the H-BEA zeolite could activate H_2 and incorporate hydrogen into the products with only minimal effect on the high selectivity to C_4 and C_7 hydrocarbons. To do so, we postulated that the metal would have to possess the following properties: (1) H_2 activation at temperatures relevant to DME homologation, (2) formation of stable ion-exchanged species within the H-BEA zeolite, (3) kinetically slow alkene hydrogenation to prevent removal of reactive alkene intermediates from the chain growth pathway, and (4) alkane dehydrogenation, enabling alkanes to be reincorporated into the chain growth pathway and indicating that H_2 could be activated in the reverse reaction. For these reasons, first-row transition metals are an attractive target, especially Cu. The key objectives of this work were to determine the effect of Cu modification on the activation and incorporation of H_2 during DME homologation and to elucidate the role of the Cu sites on H atom management.

Herein, we describe the physical, chemical, and catalytic properties of a Cu-modified H-BEA catalyst for the selective homologation of DME to hydrocarbons at 200 °C. The Cu/BEA material was characterized by X-ray diffraction (XRD), transmission electron microscopy (TEM), and X-ray absorption spectroscopy (XAS). The acid sites on Cu/BEA were investigated using NH_3 temperature-programmed desorption (TPD) and pyridine adsorption diffuse-reflectance FT-IR spectroscopy (py-DRIFTS) and compared to the parent H-BEA catalyst. The catalytic properties of Cu/BEA were tested for DME homologation both with and without H_2 cofeed, and the discharged catalysts were analyzed for residual alkylated aromatics using NMR spectroscopy. Further, H−D exchange and isobutane dehydrogenation experiments were performed to investigate the role of ionic versus metallic Cu species on the observed catalytic reactivity.

2. EXPERIMENTAL SECTION

2.1. Catalyst Preparation. Beta zeolite (BEA) having a SiO_2/Al_2O_3 ratio of 27 was obtained in ammonium form from Tosoh. The NH_4-BEA powder was used as received and had a particle/agglomerate size range of 45−125 μm. For Cu/BEA catalysts, an aqueous solution of $Cu(NO_3)_2{\cdot}2.5H_2O$ (0.961 g in 9 mL of deionized water) was added dropwise to powdered NH_4-BEA (4.95 g) to reach the incipient wetness point. The slurry was briefly mixed and then dried in an oven at 50 °C overnight to give Cu-NH_4-BEA. The targeted Cu loading was 5 wt %, and the actual measured loading (by elemental analysis) was 4.3 wt %. The measured weight loading corresponds to ∼60% of the theoretical ion-exchange capacity of the parent NH_4-BEA. A 5% Cu/SiO_2 control sample was also prepared by the analogous incipient wetness method by adding $Cu(NO_3)_2{\cdot}2.5H_2O$ (0.92 g in 27 mL of water) to silica (4.75 g, Sipernat-50, Evonik: particle size 50 μm). The measured Cu loading was 5.3 wt %.

The NH_4-BEA and Cu-NH_4-BEA catalysts were activated prior to characterization and catalytic testing. The NH_4-BEA catalyst was activated in a flowing oxidizing mixture (air, 1% O_2/He, or 10% O_2/Ar depending upon the experiment) with heating to 500 °C at 2 °C/min. The catalyst was then held at 500 °C for a minimum of 5 h. This procedure was recommended by the supplier and converted the BEA from the ammonium form to the proton form. This catalyst will be denoted as H-BEA. The Cu-NH_4-BEA catalyst was activated as described for NH_4-BEA (denoted ox-Cu/BEA). In some cases, this material was cooled to 300 °C directly after activation and exposed to flowing H_2 for a minimum of 2 h to reduce Cu (denoted red-Cu/BEA).

2.2. Catalyst Characterization. *2.2.1. Elemental Analysis.* Elemental analysis of Cu was determined by Galbraith Laboratories, Inc. (Knoxville, TN) using inductively coupled plasma atomic emission spectroscopy.

2.2.2. X-ray Diffraction. Powder X-ray diffraction data were collected using a Rigaku Ultima IV diffractometer with a Cu Kα source. Diffractograms were collected in the 2θ range of 10−60° at a scan rate of 2°/min. Samples (10−20 mg) were supported on a glass sample holder with a 0.2 mm recessed sample area and were pressed into the recession with a glass slide to obtain a uniform z-axis height. Cu and CuO crystallite sizes were calculated using the Scherrer equation.

2.2.3. Transmission Electron Microscopy. TEM was performed on red-Cu/BEA on an FEI G20 Tecnai TEM operating at 200 kV. Following reduction, a sample of the red-Cu/BEA was dispersed in anhydrous toluene under air-free conditions and dropped onto a carbon-coated Cu mesh grid. Air exposure was minimized prior to TEM imaging.

2.2.4. H_2 Temperature-Programmed Reduction. Temperature-programmed reduction (TPR) experiments were carried out in a U-shaped quartz tube at atmospheric pressure. The reactor was loaded with a mixture of 50 mg of Cu-NH_4-BEA catalysts and 300 mg of quartz chips (30−40 mesh). The catalyst sample was activated by heating to 500 °C at 2 °C/min and holding at 500 °C for 2 h in flowing 1% O_2/He (20 mL/min). The sample was then cooled to room temperature in flowing He before heating to 600 °C at 10 °C/min in 2% H_2/He (20.4 mL/min). The gas composition was monitored by a mass spectrometer.

2.2.5. Total Acid Site Titration: NH_3 TPD. The total number of acid sites were determined using NH_3 TPD on an Altamira Instruments AMI-390 system with gas flow rates of 25 mL/min. Catalyst samples (ca. 250 mg) were loaded into a 1/2 in. quartz U-tube reactor and held as a fixed bed between plugs of quartz wool. Samples were calcined in flowing 10% O_2/Ar at 2 °C/min to 500 °C and then held at this temperature for 5 h. For the red-Cu/BEA catalyst, the sample was subsequently reduced in flowing 10% H_2/Ar at 300 °C for 5 h. The samples were cooled to 120 °C in flowing He and then saturated with flowing 10% NH_3/He for 30 min. Excess and/or physisorbed NH_3 was removed by holding the samples at 120 °C in flowing He for 1 h. TPD of NH_3 was performed by heating the sample from 120 to 500 °C at 30 °C/min. The temperature was then held at 500 °C for 30 min to allow any remaining NH_3 to desorb without increasing the temperature above the 500 °C activation temperature, as recommended elsewhere.[8] Desorbed NH_3 was measured with a thermal conductivity detector, and calibration was performed after each experiment by introducing five pulses of 10% NH_3/He from a 5 mL sample loop into a stream of flowing He.

2.2.6. Brønsted and Lewis Acid Site Titration: Pyridine DRIFTS. The relative amounts of Lewis and Brønsted acid sites were determined by py-DRIFTS using a Thermo Nicolet iS50 FT-IR spectrometer operating at 4 cm^{-1} resolution with a Harrick praying mantis attachment and Si windows operated at ambient pressure. As-prepared materials were activated in situ

DOI: 10.1021/cs501876w
ACS Catal. 2015, 5, 1794−1803

at 500 °C in flowing air (50 mL/min, 2 °C/min from ambient, 10 h soak) and then purged with flowing N_2 at 150 °C for 30 min. For red-Cu/BEA, the catalyst was reduced in 5% H_2 at 300 °C for 4 h. After pretreatment, the sample was held at 150 °C, and saturated pyridine vapor was introduced with N_2 for 5 min. The sample was then heated to 300 °C under flowing N_2 (or 5% H_2 for red-Cu/BEA) to remove excess and/or physisorbed pyridine. The absorption peaks at 1545 cm^{-1} (Brønsted) and 1445 cm^{-1} (Lewis) and their relative absorption coefficients ($\varepsilon_B/\varepsilon_L$ = 0.76) were used to determine the relative Brønsted/Lewis acid site ratios, per common practice.[9,10]

2.2.7. Quantification of Hexamethylbenzene: ^1H and ^2H NMR. The amount of HMB remaining on the catalyst after reaction was determined using ^1H NMR spectroscopy. Solution-phase ^1H and ^2H NMR spectra were recorded using a Varian Inova 400 MHz spectrometer. Post-reaction catalyst samples (ca. 100 mg) were combined with solvent (0.7 mL of $CDCl_3$ for ^1H; 0.7 mL of $CHCl_3$ for ^2H) and internal standard (10 μL CH_2Cl_2) in a sealed NMR tube. The tube was shaken briefly and analyzed for solubilized organics.

2.2.8. H−D Exchange. H−D exchange experiments were carried out in a U-shaped quartz tube at atmospheric pressure. Samples of as-prepared materials (ca. 50 mg) were converted to the proton form in situ by heating at 2 °C/min to 500 °C and holding for 2 h under flowing 1% O_2/He (20 mL/min). For the red-Cu/BEA catalyst, the sample was then reduced at 300 °C for 2 h under flowing H_2 (20 mL/min, undiluted, 99.999%). The samples were cooled to room temperature in He and then heated at 10 °C/min to 800 °C in flowing D_2 (Matheson, 99.999%) at 20 mL/min. A mass spectrometer was used to measure the effluent gas composition.

2.2.9. Isobutane Dehydrogenation. The dehydrogenation of isobutane was performed in a U-shaped quartz tube at atmospheric pressure. The as-prepared catalyst (ca. 100 mg) was mixed with 300 mg of quartz chips (30−40 mesh) and then loosely packed into the reactor with quartz wool. Catalysts were activated by heating to 500 °C at 2 °C/min in flowing 1% O_2/He (20 mL/min) and holding at 500 °C for 2 h. For red-Cu/BEA, the catalyst was reduced at 300 °C for 2 h in flowing H_2 (20 mL/min, undiluted, 99.999%). After pretreatment, the catalyst sample was heated from room temperature to 600 °C at 10 °C/min in 1% isobutene/He at a flow rate of 5 mL/min. A mass spectrometer was used to monitor the reaction products.

2.2.10. X-ray Absorption Spectroscopy. X-ray absorption measurements were acquired on the bending magnet beamline (10-BM) of the Materials Research Collaborative Access Team (MRCAT) at the Advanced Photon Source, Argonne National Laboratory. Photon energies were selected using a water-cooled, double-crystal Si(111) monochromator, which was detuned by approximately 50% to reduce harmonic reflections. Measurements were made in transmission mode, and data points were acquired in three separate regions (energies relative to the elemental Cu K edge): a pre-edge region (−250 to −30 eV, step size 10 eV, dwell time 0.25 s), the X-ray absorption near-edge structure (XANES) region (−30 to +30 eV, step size 0.5 eV, dwell time 0.25 s), and the extended X-ray absorption fine structure (EXAFS) region (to 13 $Å^{-1}$, step size 0.07 $Å^{-1}$, dwell time 1 s). The ionization chambers were optimized for the maximum current with linear response (~10^{10} photons detected/s) with 10% absorption (93% N_2 and 7% He) in the incident ion chamber and 70% absorption (50% N_2 and 50% Ar) in the transmission detector. A Cu foil spectrum (edge energy 8979.0 eV) was acquired simultaneously with each measurement for energy calibration.

Catalysts were treated in a continuous-flow reactor, which consisted of a quartz tube (1 in. o.d., 10 in. length) sealed with Kapton windows by two Ultra-Torr fittings. Ball valves were welded to each Ultra-Torr fitting and served as the gas inlet and outlet. An internal K type thermocouple (Omega) was placed against the catalyst sample holder to monitor temperature. Catalyst samples were pressed into a cylindrical sample holder consisting of six wells, forming a self-supporting wafer. The catalyst loading was predetermined to ensure an absorbance (μ_x) of approximately 1.0. The catalysts were treated at the indicated temperature in air or H_2 and cooled to room temperature before obtaining spectra to minimize contributions due to thermal effects. XANES and EXAFS spectra taken at high temperature (500 and 300 °C) were similar to those at room temperature except for the thermal disorder in the EXAFS. Traces of oxygen and moisture in the He were removed by means of a purifier (Matheson PUR-Gas Triple Purifier Cartridge).

The edge energy of the XANES spectrum was determined from the inflection point in the leading edge: i.e., the maximum in the first derivative of the XANES spectrum. Experimental Cu−O phase shift and backscattering amplitude were obtained from the reference compound copper(II) acetylacetonate ($Cu(acac)_2$; 4 Cu−O at 1.92 Å) and used to fit the data.[11] Background removal and normalization procedures were carried out using standard methods. Standard procedures for normalization and background subtraction were performed using WinXAS 3.2 software.[12] The coordination parameters were obtained by a least-squares fit in R space of the nearest-neighbor, k^2-weighted Fourier transform data.

2.3. Dimethyl Ether Homologation Catalytic Measurements. Catalyst powders (~0.6 g) were diluted with low-surface-area, inert silicon carbide in a 1:6 mass ratio of catalyst to diluent to prevent channeling, avoid problems with axial dispersion, and minimize temperature gradients in the bed. The catalysts were loaded into a stainless steel tubular packed bed reactor and positioned within the isothermal zone using quartz chips and quartz wool. A four-point thermocouple positioned within the catalyst bed was used to monitor reaction temperature. The reaction temperature during an experiment was maintained within ±0.5 °C of the set point. Prior to reaction rate measurements, the catalysts were activated by ramping from room temperature to 500 °C at 2 °C/min in flowing dry air at 150 mL min^{-1} g_{cat}^{-1} and holding at 500 °C for 10 h. For the red-Cu/BEA catalyst, the sample was cooled to 300 °C in inert gas following air activation at 500 °C, and then exposed to H_2 flowing at 150 mL min^{-1} g_{cat}^{-1}. The catalyst was held at 300 °C in H_2 for 5 h before cooling to the reaction temperature. A physical mixture of 5% Cu/SiO_2 and NH_4-BEA (0.3 g of each material) was also tested (denoted H-BEA-Cu/SiO_2) and was activated using the same procedure as the red-Cu/BEA catalyst.

All reactions were performed at 200 °C and atmospheric pressure, and DME conversion was maintained below 20%. Two feed mixtures were tested: (1) 7.1 mL/min of DME and 4.9 mL/min of Ar (60 mol % DME and 40 mol % Ar) and (2) 7.1 mL/min of DME, 7.1 mL/min of H_2, and 1 mL/min of Ar (47 mol % DME, 47 mol % H_2, and 6 mol % Ar). The reaction conditions without H_2 cofeed were similar to those tested by Ahn et al.[4] Single-component gases were fed to the reactor via calibrated Brooks thermal mass flow controllers. Reactor inlet

DOI: 10.1021/cs501876w
ACS Catal. 2015, 5, 1794−1803

and outlet gases were sampled through heated (170 °C) lines to an Agilent 7890 GC instrument equipped with a flame ionization detector for analysis of oxygenates and hydrocarbons and two thermal conductivity detectors for analysis of permanent gases and water. GC responses for reactants and products were calibrated using Scott Master Class gas standards and gravimetrically prepared liquid standards. The effluent was sampled every 45 min. Catalyst performance was evaluated solely from inlet flow and GC measurements using Ar as an internal standard. Hydrocarbon production rates were normalized by the total number of acid sites as determined by NH_3-TPD.

3. RESULTS AND DISCUSSION

3.1. Structural and Chemical Characterization of the Cu Species. The H-BEA and Cu/BEA catalysts were characterized using a suite of bulk- and surface-sensitive techniques to probe their chemical and structural properties. The bulk crystal structure of H-BEA matched the known reported structure for BEA zeolite,[13] as confirmed by XRD (Figure S1 in the Supporting Information). The addition of Cu resulted in CuO domains (crystallite size of 30 nm) for ox-Cu/BEA and metallic Cu domains (crystallite size of 43 nm) for red-Cu/BEA. The formation of large CuO domains upon air oxidation at 500 °C is due to the high Cu loading and the deposition of Cu via incipient wetness (instead of ion exchange methods). However, it is likely that a small amount of Cu was ion-exchanged into the BEA pores during impregnation. The H_2 TPR profile of ox-Cu/BEA showed only one strong peak at approximately 255 °C, attributed to the one-step reduction of CuO to metallic Cu (Figure S2 in the Supporting Information).[14−16] TEM images confirmed the presence of metallic Cu nanoparticles, as shown in Figure 1. The nanoparticles were polydisperse with

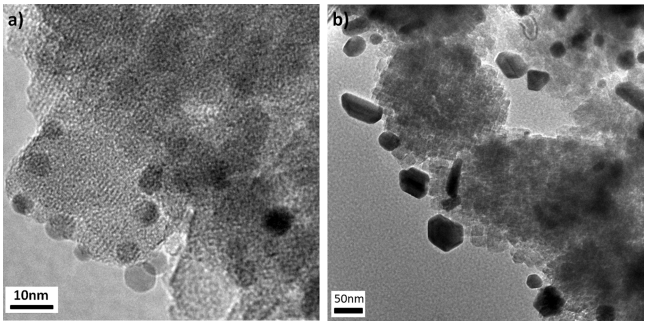

Figure 1. TEM images showing the distribution of (a) small (<10 nm) and (b) larger (>20 nm) metallic Cu particles associated with red-Cu/BEA.

diameters ranging from 2 to 60 nm. It should be noted that no effort was made to control the size of these metallic nanoparticles.

Figure 2a shows the XANES spectra collected at the Cu K edge for the as-synthesized Cu-NH_4-BEA in air at room temperature, ox-Cu/BEA, red-Cu/BEA, and Cu foil. The ox-Cu/BEA sample has a small pre-edge feature characteristic of Cu(II), while the edge energy of the red-Cu/BEA catalyst is identical with that of Cu foil. The XANES spectrum of the reduced sample, however, has a shape slightly different from that of Cu foil, consistent with a small fraction of oxidized Cu.

The XANES spectra were fit using a linear combination of Cu(0), Cu(I), and Cu(II) standards to estimate the relative concentrations of each phase. Cu foil was used as the standard for Cu(0), Cu(I)-SSZ-13 (Cu(I)-zeolite) and Cu_2O were used as Cu(I) references, and Cu(II)-SSZ-13 (Cu(II)-zeolite) and CuO were used as Cu(II) references.[17] The reference spectra for the standards are provided in Figure S3 in the Supporting Information. For ox-Cu/BEA, the best fit was a mixture of CuO and Cu(II)-zeolite with relative concentrations of 45% and 55%, respectively. Inclusion of Cu(I) standards gave similar quality fits but only amounted to less than 5% Cu(I). For red-Cu/BEA, there is a high fraction of metallic Cu (∼86%) but a residual fraction that is unreduced. The best fit suggests that the unreduced portion is a mixture of Cu(I)-zeolite (4%) and Cu(II)-zeolite (10%). The reduction of Cu(II) ions within zeolite pores is reported to occur stepwise, Cu(II) → Cu(I) → Cu(0), and the temperatures at which these reductions occur are dependent upon the zeolite type, Cu ion location within the pore, Si/Al ratio, and ion exchange level of Cu.[18−23] For Cu-BEA, the reductions of Cu(II) to Cu(I) and of Cu(I) to Cu(0) have been reported to occur at 200 and 390 °C, respectively.[23] This finding would suggest that all of the ionic Cu in the red-Cu/BEA sample should be present as Cu(I); however, ∼10% of the Cu remained as Cu(II). The presence of Cu(II) in the red-Cu/BEA sample is likely due to the low concentration of ion-exchanged Cu (the fraction of Cu present as Cu(II) in the red-Cu/BEA sample corresponds to 8% of the ion exchange capacity of the parent NH_4-BEA), as it has been reported that the Cu ion reduction temperature increases with decreased Cu loading.[22,23]

The k^2-weighted magnitude of the Fourier transform of the red-Cu/BEA sample is shown in Figure 2b along with that of the Cu foil. In the region typical of Cu−O bonds (i.e., ∼1.7 Å), there is a small feature; however, this feature is too small to fit directly since the scattering from metallic Cu is much larger than that of Cu−O. In order to fit the Cu−O contribution, the Cu−Cu coordination was first determined (9.5 at 2.54 Å). By scaling ψ from the Cu foil to the Cu−Cu coordination number in the catalyst, the metallic Cu scattering was subtracted from the red-Cu/BEA spectrum, leaving only the Cu−O scattering contribution. The Cu−O coordination number was determined to be 1.3 with a bond distance of 1.92 Å (Table S1 in the Supporting Information). The presence of oxidized Cu and the low Cu−O coordination number suggest the presence of ion-exchanged Lewis acidic cationic Cu.

3.2. Acid Site Characterization. Acid site densities were determined by NH_3-TPD (Figure 3a) and are given in Table 1. The H-BEA TPD profile resembled literature reports,[24,25] exhibiting two distinct desorption peaks at 334 and 470 °C, attributed to weak and strong acid sites, respectively. The addition of Cu resulted in an increase in the total number of acid sites and additional features in the TPD profile in comparison to H-BEA, specifically a low-temperature desorption peak at ∼275 °C. The ox-Cu/BEA profile also exhibited a sharp peak at 342 °C, attributed to the decomposition of a Cu ammonia complex (i.e., NH_3 bonded at Cu cationic species).[26,27] The lack of this sharp peak for the red-Cu/BEA sample is in agreement with the XAS results, showing that only a small amount of cationic Cu was present for the red-Cu/BEA sample.

Py-DRIFTS was performed to investigate the acidic character (i.e., Lewis vs Brønsted) of the catalysts.[9] Figure 3b presents the IR spectra between 1400 and 1650 cm^{-1} for H-BEA, ox-Cu/BEA, and red-Cu/BEA after adsorption of pyridine at 150 °C followed by purging with N_2. The peaks at 1545, 1490, and ∼1450 cm^{-1} correspond to pyridine bound to Brønsted sites, Brønsted and Lewis sites, and Lewis sites, respectively.

DOI: 10.1021/cs501876w
ACS Catal. 2015, 5, 1794−1803

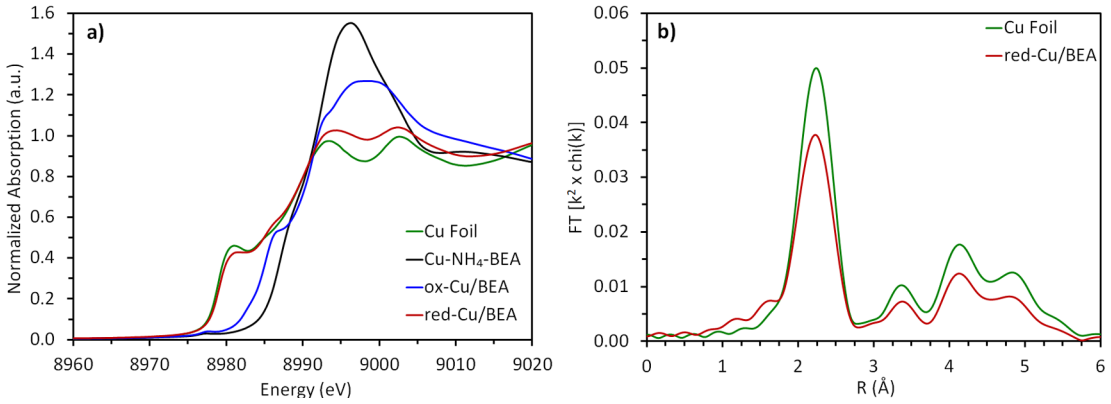

Figure 2. X-ray absorption spectra for as-prepared Cu/BEA following various treatments: (a) XANES and (b) EXAFS. Reference spectra for a Cu foil are provided for comparison.

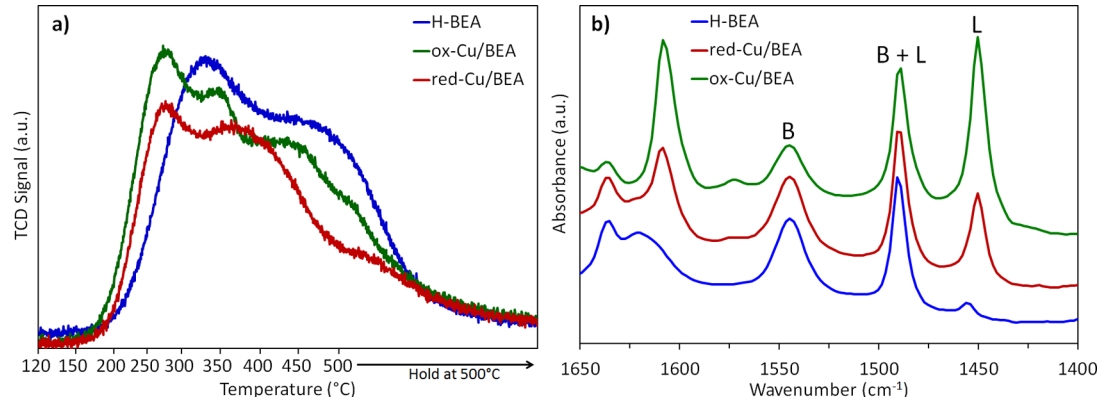

Figure 3. Surface acidity characterization for the H-BEA, ox-Cu/BEA, and red-Cu/BEA catalysts using (a) NH_3-TPD and (b) py-DRIFTS.

Table 1. Acidity Results from NH_3-TPD and py-DRIFTS

					NH_3 desorption peak temp (°C)			
catalyst	total acid site[a] (μmol/g)	Brønsted/Lewis ratio[b]	Brønsted acid site (μmol/g)	Lewis acid site (μmol/g)	1	2	3	4
H-BEA	1642	16.8	1550	92	334	470		
ox-Cu/BEA	2058	0.6	772	1286	277	342	427	500[c]
red-Cu/BEA	1918	2.3	1337	581	275	371	500[c]	

[a]Total acid site density determined from NH_3-TPD. The catalyst sample weight after the activation procedure was used to normalize the results. [b]Brønsted/Lewis acid site ratio was determined from py-DRIFTS. [c]Desorption peak occurred during 30 min hold at 500 °C.

When the integrated areas of the peaks at 1545 and 1450 cm^{-1} are compared, the relative ratio of Brønsted to Lewis sites can be determined (assuming the same extinction coefficient for py-Al and py-Cu species at 1450 cm^{-1}).[9,28−30] The Brønsted/Lewis ratios for H-BEA, ox-Cu/BEA, and red-Cu/BEA were 16.8, 0.6, and 2.3, respectively. The addition of Cu decreased the density of Brønsted sites in comparison to H-BEA, due to conversion of Brønsted sites into Lewis sites by ion-exchanged Cu and pore blocking by large CuO and Cu domains. A small peak at 1575 cm^{-1} was also observed for the Cu-containing samples (more prominent for ox-Cu/BEA) and has been attributed to pyridine adsorption to a Cu(II)−OH site.[30−32] Cu provided an additional Lewis site (1608 cm^{-1}), weaker than tetrahedral Al(III) (1635 cm^{-1}) and comparable in strength to octahedral Al(III) (1612 cm^{-1}).[33] The intensity of this Cu-based Lewis site at 1608 cm^{-1} decreased after reduction, consistent with Brønsted/Lewis ratios determined from peak area integrations at 1545 and 1450 cm^{-1}. These results demonstrate the significant increase in Lewis acidity with the presence of Cu, suggesting Cu(I) or Cu(II) sites, which is in good agreement with the NH_3-TPD and XAS fits.

3.3. Catalytic Testing and Mechanistic Studies.

3.3.1. Dimethyl Ether Homologation. The catalytic performance of ox-Cu/BEA, red-Cu/BEA, and a physical mixture of Cu/SiO_2 with H-BEA (H-BEA-Cu/SiO_2) is compared to that of the parent H-BEA in Figure 4. The initial C−C bond formation for DME homologation may be facilitated by trace amounts of hydrocarbon (i.e., olefin) contaminants in the DME feed. The C_1−C_7 hydrocarbon production rate for H-BEA without H_2 cofeed was similar to that with H_2 cofeed (Figure 4a). At 1.6 h time on stream (TOS), the H-BEA catalyst exhibited a hydrocarbon production rate of 827 μmol C mol_{site}^{-1} s^{-1}. This value is slightly higher than that reported by Ahn et al. under similar conditions (740 μmol C mol_{Al}^{-1} s^{-1} at 1.2 h TOS).[4] This difference may be due to slightly different SiO_2/Al_2O_3 ratios of the parent BEA materials and acid site determination methods (theoretical Al density vs experimental NH_3-TPD). The red-Cu/BEA catalyst without H_2 in the feed exhibited a

DOI: 10.1021/cs501876w
ACS Catal. 2015, 5, 1794−1803

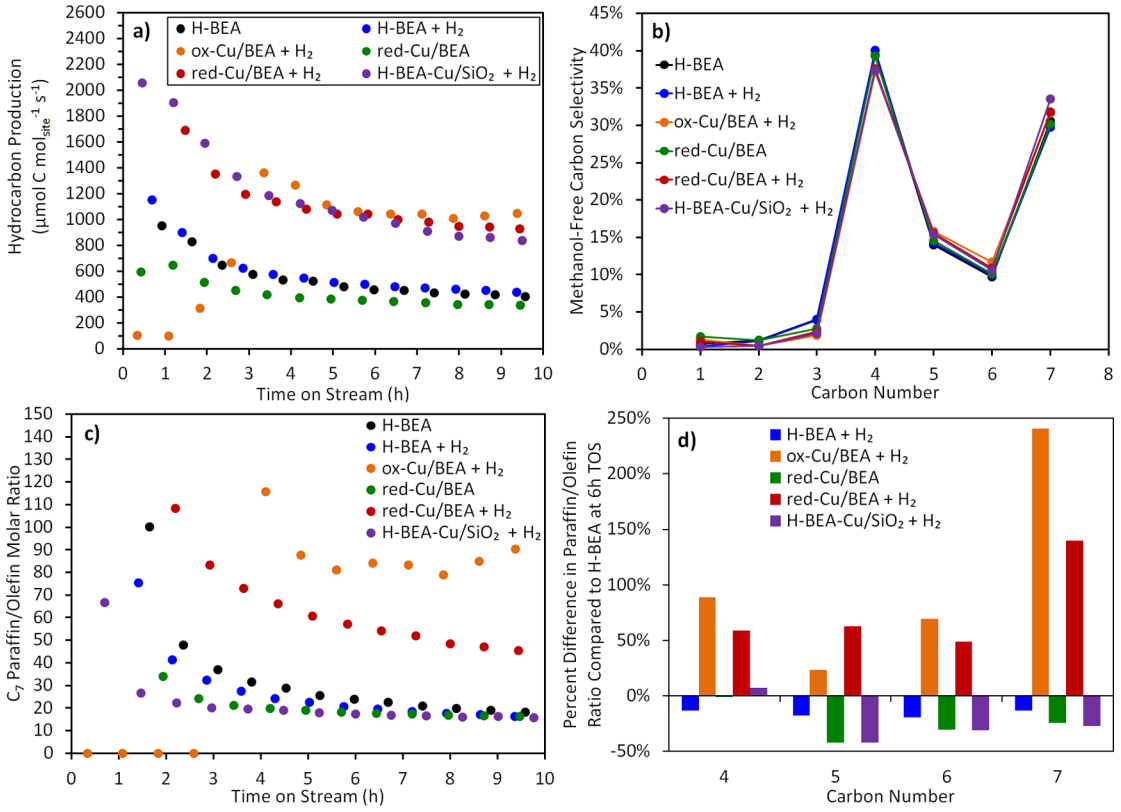

Figure 4. DME homologation rates and product selectivities: (a) hydrocarbon production rates; (b) methanol-free carbon selectivities at 6 h TOS; (c) C_7 paraffin/olefin molar ratios; (d) percent difference in C_4−C_7 paraffin/olefin molar ratios in comparison to H-BEA at 6 h TOS. For H-BEA-Cu/SiO_2, the hydrocarbon production rate in (a) is based on the number of acid sites present on the H-BEA. The reactions were performed using 0.6 g of catalyst at 200 °C and ∼1 atm and a feed flow rate of either 12 mL/min (60 mol % DME, 40 mol % Ar) for experiments without H_2 cofeed or 15.2 mL/min (47 mol % DME, 47 mol % H_2, 6 mol % Ar) for experiments with H_2 cofeed.

hydrocarbon production rate slightly lower than that of H-BEA, while ox-Cu/BEA without H_2 showed no detectable hydrocarbon production. We hypothesize that this lack of activity for ox-Cu/BEA may be due to Cu ions inhibiting the formation of surface methoxides or alkoxides by (1) the formation of Cu−OH species (as discussed in section 3.2) that are responsible for the observed Brønsted acidity and (2) the elimination of Brønsted −OH groups via ion exchange. However, when H_2 was included in the feed, the production rate for red-Cu/BEA was ∼2 times greater than that for H-BEA on both a gravimetric and per site basis (1689 μmol C mol_{site}^{-1} s^{-1} at 1.5 h TOS). A similar increase in performance was also observed for the physical mixture of Cu/SiO_2 and H-BEA, suggesting that metallic Cu may be responsible for the improved production rate. In further support, the presence of H_2 for ox-Cu/BEA resulted in an increase in hydrocarbon productivity between 1 and 3 h TOS (achieving rates similar to red-Cu/BEA), likely due to reduction of CuO to metallic Cu.

The significant increase in productivity for the red-Cu/BEA catalyst in the presence of H_2 appeared to have a negligible effect on the methanol-free carbon selectivity, as shown in Figure 4b. As observed by Ahn et al.,[4] high selectivity was achieved to both C_4 and C_7 hydrocarbons. The C_7 selectivities at 6 h TOS for H-BEA, H-BEA + H_2, ox-Cu/BEA + H_2, red-Cu/BEA, red-Cu/BEA + H_2, and H-BEA-Cu/SiO_2 + H_2 were 31%, 30%, 32%, 30%, 32%, and 33%, respectively (error on measurements is ±1%). H_2 cofeed also had minimal effect on the product selectivity of H-BEA. However, Cu-containing catalysts modified the degree of product saturation in comparison to H-BEA, as shown in Figure 4c,d. The C_7 paraffin/olefin molar ratio over red-Cu/BEA + H_2 (and ox-Cu/BEA + H_2 after 3 h TOS) was more than 2.5 times greater than that of H-BEA (Figure 4c). Interestingly, the physical mixture of H-BEA and Cu/SiO_2 behaved similarly to H-BEA, suggesting minimal hydrogenation of triptene and other C_7 olefins by metallic Cu supported on SiO_2. In general, the red-Cu/BEA catalyst with H_2 cofeed yielded products with significantly increased paraffin/olefin ratios for all carbon numbers in comparison to H-BEA (Figure 4d and Figures S4 and S5 in the Supporting Information). The physical mixture of H-BEA and Cu/SiO_2 did increase paraffin/olefin ratios over H-BEA, but only for C_2 and C_3 hydrocarbons. Metallic Cu nanoparticles are known to perform olefin hydrogenation, albeit at a rate much lower than that for platinum-group metals.[34] These results suggest that (1) metallic Cu performs olefin hydrogenation of ethylene and propylene primarily, (2) the increased selectivity toward paraffins for C_4−C_7 hydrocarbons over red-Cu/BEA + H_2 was due to either close proximity of the metallic Cu to the BEA zeolite active site and/or the presence of cationic Cu within the BEA pores, and (3) the increased hydrocarbon production rate for red-Cu/BEA + H_2 and H-BEA-Cu/SiO_2 + H_2 is related to the increase in paraffin/olefin ratio for C_2 and C_3 hydrocarbons. These preliminary conclusions will be discussed in greater detail in section 3.4.

Without H_2 in the feed, red-Cu/BEA demonstrated a higher selectivity toward C_5−C_7 olefins compared to H-BEA (Figure 4c,d and Figure S4 in the Supporting Information). The paraffin/olefin ratio over red-Cu/BEA for C_5, C_6, and C_7 hydrocarbons at 6 h

DOI: 10.1021/cs501876w
ACS Catal. 2015, 5, 1794−1803

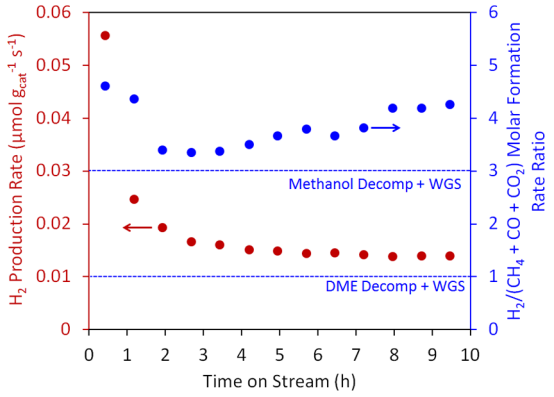

Figure 5. H_2 production rate and $H_2/(CH_4 + CO + CO_2)$ molar formation rate ratio as a function of TOS for red-Cu/BEA experiment. The dashed lines correspond to the maximum $H_2/(CH_4 + CO + CO_2)$ values achievable on the basis of only methanol decomposition-WGS or only DME decomposition-WGS. The reaction was performed using 0.6 g of catalyst at 200 °C, ~1 atm, and a feed flow rate of 12 mL/min (60 mol % DME, 40 mol % Ar).

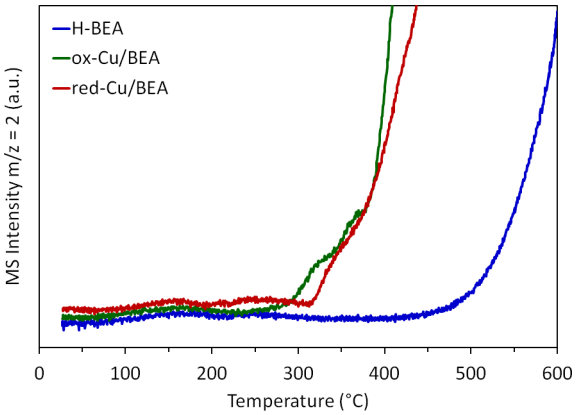

Figure 6. Hydrogen (m/z 2) evolution during isobutane dehydrogenation experiments for H-BEA, ox-Cu/BEA, and red-Cu/BEA.

TOS decreased by 41%, 31%, and 24% in comparison to H-BEA, respectively. Additionally, H_2 production was observed during DME homologation over red-Cu/BEA (Figure 5). No H_2 production was observed over H-BEA. The production of H_2 could occur via DME/methanol decomposition over metallic Cu[35] or alkane dehydrogenation over Lewis acidic cationic Cu sites.[36] The decomposition of DME would result in the formation of H_2, CH_4, and CO at a stoichiometry of 1:1:1, whereas the decomposition of methanol would produce H_2 and CO at a stoichiometry of 2:1. However, since metallic Cu is an active water-gas shift (WGS) catalyst and water is produced as a product of DME homologation, CO could also undergo WGS to produce CO_2 and H_2. Thus, assuming that H_2 is being produced only via decomposition and WGS, the maximum attainable value for a ratio of the molar formation rates of $H_2/(CH_4 + CO + CO_2)$ would be 3 for only methanol decomposition combined with WGS and 1 for only DME decomposition combined with WGS (corresponding to the dashed lines in Figure 5). The $H_2/(CH_4 + CO + CO_2)$ molar formation rate ratio is shown in Figure 5 for red-Cu/BEA, and the values were greater than 3 throughout the experiment. The high concentration of DME in the feed and the increase in CH_4 selectivity observed for red-Cu/BEA (Figure 4b; 1.7% for red-Cu/BEA vs 0.7% for H-BEA) suggest that DME decomposition likely contributed to more H_2 production than methanol decomposition. These results suggest that, while methanol/DME decomposition was occurring during DME homologation over red-Cu/BEA, it was not the only source of H_2 production; alkane dehydrogenation was also occurring.

3.3.2. Isobutane Dehydrogenation. Temperature-programmed reactions with isobutane were performed to test the dehydrogenation activity of the H-BEA, ox-Cu/BEA, and red-Cu/BEA catalysts, and the results are provided in Figure 6. H_2 evolution over H-BEA did not occur until ~500 °C, whereas it was observed at 275−300 °C for ox-Cu/BEA and red-Cu/BEA. The only products observed were H_2 and isobutylene. The similarity of the H_2 evolution onset temperatures for ox-Cu/BEA and red-Cu/BEA suggests that the low-temperature dehydrogenation activity is most likely attributed to cationic Cu species (potentially in combination with Brønsted acid sites), not metallic Cu sites.

Alkane dehydrogenation requires C−H bond activation (i.e., hydrogen abstraction) and recombinative desorption of hydrogen atoms to form H_2. Simonetti et al. demonstrated that H-BEA can dehydrogenate branched alkanes (i.e., isobutane) via hydride-transfer reactions with surface alkoxides at 200 °C.[6] However, isobutane dehydrogenation over H-BEA was not observed until approximately 500 °C (Figure 6). The reported rate-limiting step for alkane dehydrogenation over zeolites is hydrogen recombination.[37] These results suggest that cationic Cu species catalyze recombinative hydrogen desorption, similar to ion-exchanged Ga in Ga/H-ZSM5 during propane aromatization.[37−39] Thus, for DME homologation over red-Cu/BEA without cofed H_2, hydrogen abstracted from branched alkanes can either be transferred to alkoxides on the zeolite surface via a bimolecular hydride-transfer step[6] or recombine and desorb on cationic Cu species. As this result supports the formation of cationic Cu−H_x or CuO_x−H species under reaction conditions, cofed H_2 likely dissociates on these cationic Cu species, resulting in hydrogenation of olefins or hydrogen transfer to surface alkoxides. This proposed phenomenon agrees with the trend in paraffin/olefin ratios observed for red-Cu/BEA + H_2 in comparison to H-BEA-Cu/SiO_2 + H_2 (Figure 4d and Figure S5 in the Supporting Information), which suggests that cationic Cu species are required to achieve an increase in C_4−C_7 paraffin/olefin ratios. The effect of cationic Cu species on C−H activation still needs to be determined but is outside the scope of this paper.

3.3.3. H−D Exchange and D_2 Incorporation. Due to the significant increases in productivity and paraffin selectivity for red-Cu/BEA + H_2, we probed the activation of H_2 over H-BEA, ox-Cu/BEA, and red-Cu/BEA using H−D exchange experiments. Figure 7 shows the evolution of HD during isotopic exchange of D_2 with hydrogen atoms over the activated catalysts. The hydrogen comes from −OH groups on the catalyst surface, including Brønsted protons from zeolitic-bridged −OH groups, silanols, or −OH groups at extraframework Al and Cu atoms (e.g., Cu(II)−OH). The red-Cu/BEA catalyst was capable of activating D_2 and evolving HD at a significantly lower temperature than H-BEA. The maximum rate of HD evolution was observed at ~180 °C for red-Cu/BEA and ~500 °C for H-BEA. The ox-Cu/BEA sample also exhibited a low-temperature peak for HD evolution (~200 °C); however, D_2O production was also observed at this temperature, indicating that CuO particles were reduced to metallic Cu from the D_2 in the feed (in agreement with DME homologation results

DOI: 10.1021/cs501876w
ACS Catal. 2015, 5, 1794−1803

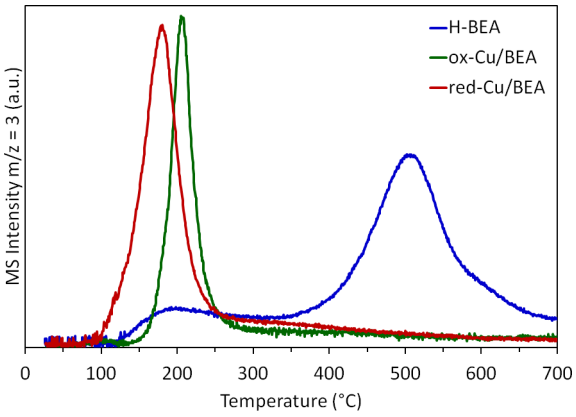

Figure 7. HD (m/z 3) evolution during H−D exchange experiments for H-BEA, ox-Cu/BEA, and red-Cu/BEA.

showing an increase in hydrocarbon productivity after 3 h TOS). The total amounts of HD evolved (i.e., the area under the curve) were nearly identical for H-BEA and red-Cu/BEA, suggesting that the D_2 activated by the Cu can reach all of the H atoms present within the zeolite. The total amount of HD evolved for ox-Cu/BEA was approximately 65% of that for H-BEA. Proton mobility and H_2 spillover on aluminosilicate surfaces is a debated topic in the literature.[40] It has been reported that acidic protons within zeolites can be mobile at elevated temperatures, and their mobility may be enhanced by the presence of H_2O.[41−43] The spillover of H_2 onto a defect-free zeolite surface is believed to be energetically impossible; however, H_2 spillover onto zeolite surfaces with defects or carbonaceous deposits may be possible.[40] Recently, a study by Im et al. demonstrated experimentally and theoretically that H_2 spillover can occur on an aluminosilicate surface at DME homologation temperatures via a defect generation−annihilation pathway.[44] Although H−D exchange is not direct proof of H_2 spillover, these results indicate that activated hydrogen is available during DME homologation over red-Cu/BEA for hydrogen transfer or hydrogenation reactions that may occur at defect sites, cationic Cu sites, and metallic Cu sites or on carbonaceous deposits.

The activation and incorporation of H_2 was further explored through isotopically labeled experiments. D_2 was cofed with DME over H-BEA and red-Cu/BEA, and the incorporation of deuterium into the hydrocarbon products was monitored using mass spectrometry. The mass spectra for triptane collected at 6 h TOS are shown in Figure 8. When H_2 is replaced with D_2 over H-BEA, there is no change in the resulting mass spectrum for triptane. In contrast, over red-Cu/BEA, significant incorporation of deuterium into the desired product was observed. This deuterium incorporation was observed for all representative products, including HMB (Figures S6−S8 in the Supporting Information).

3.4. Mechanistic Interpretations. As discussed earlier, the direct homologation of DME to alkanes is hydrogen deficient. The necessary hydrogen atoms are provided by the formation of alkylated aromatic byproducts, such as HMB. For the red-Cu/BEA catalyst, hydrogen atoms are provided by the activation of gaseous H_2 and are incorporated into the hydrocarbon products, suggesting that the formation of alkylated aromatics may be reduced. It has been reported that the conversion of methanol to hydrocarbons occurs via a dual catalytic cycle of olefin and aromatic methylation[3,45,46] and that

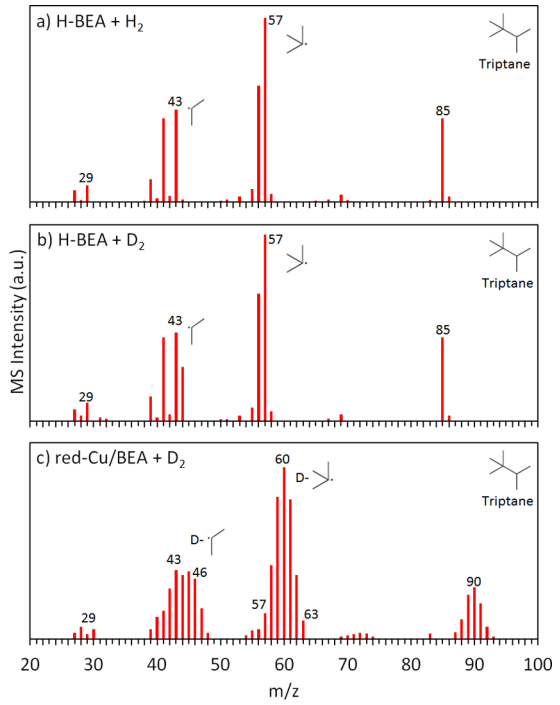

Figure 8. Mass spectra for triptane collected at 6 h TOS from (a) H-BEA + H_2, (b) H-BEA + D_2, and (c) red-Cu/BEA + D_2 experiments. The reactions were performed using 0.6 g of catalyst at 200 °C, ∼1 atm, and a feed flow rate of 15.2 mL/min (47 mol % DME, 47 mol % H_2 or D_2, 6 mol % Ar).

the relative propagation of the olefin and aromatic cycles can be determined by calculating the ratio of ethylene to 2-methylbutane and 2-methylbutene (2MB) in the products.[3,46]

Accordingly, we determined the ratios of the molar formation rates of ethane and ethylene to 2MB (r_{C_2}/r_{2MB}) and the ratios of carbon present in HMB to carbon present in hydrocarbons (C_{HMB}/C_{HC}) to probe the effect of H_2 introduction on (1) the relative rates of production of hydrocarbons from the aromatic and olefin cycles and (2) alkyl-aromatic formation via the olefin catalytic cycle. Table 2 provides these ratios for the catalysts with and without cofed H_2. Ethane was included with ethylene

Table 2. Effect of Cu Addition on Product Selectivity

experiment[a]	r_{C_2}/r_{2MB}[b]	r_{C_2}/r_{2MB}[c]	C_{HMB}/C_{HC}[d]
H-BEA	0.23	0.16	0.12
H-BEA + H_2	0.21	0.15	0.07
ox-Cu/BEA + H_2	0.08	0.07	0.03
red-Cu/BEA	0.24	0.24	0.14
red-Cu/BEA + H_2	0.08	0.08	0.04
H-BEA-Cu/SiO_2 + H_2	0.08	0.09	0.03

[a]The reactions were performed using 0.6 g of catalyst at 200 °C, ∼1 atm, and a feed flow rate of either 12 mL/min (60 mol % DME, 40 mol % Ar) for experiments without H_2 cofeed or 15.2 mL/min (47 mol % DME, 47 mol % H_2, 6 mol % Ar) for experiments with H_2 cofeed. [b]Ratio of molar formation rate of ethane and ethylene to molar formation rate of 2-methylbutane and 2-methylbutenes at 6 h TOS. [c]Ratio of molar formation rate of ethane and ethylene to molar formation rate of 2-methylbutane and 2-methylbutenes at a DME conversion of 11% (different TOS). [d]Ratio of total carbon present in HMB to total carbon in C_1−C_7 hydrocarbons produced over an entire experiment.

DOI: 10.1021/cs501876w
ACS Catal. 2015, 5, 1794−1803

due to probable olefin hydrogenation over metallic Cu. Calculated either at the same TOS or at the same conversion, red-Cu/BEA + H_2 and H-BEA-Cu/SiO_2 + H_2 exhibited lower r_{C_2}/r_{2MB} ratios than H-BEA, suggesting that the addition of metallic Cu promoted propagation of the olefin cycle. This shift was further confirmed by the C_{HMB}/C_{HC} ratios. Red-Cu/BEA + H_2 exhibited a C_{HMB}/C_{HC} ratio of 0.04 in comparison to that of 0.12 for H-BEA. The decreased HMB production for red-Cu/BEA + H_2 is not likely due to hydrogenation of HMB on metallic Cu, as supported metallic Cu catalysts have been reported to be inactive for aromatic ring hydrogenation under similar reaction conditions.[47,48] As discussed previously, the ox-Cu/BEA + H_2 behaved similarly to red-Cu/BEA + H_2 as the cofed H_2 resulted in the reduction of CuO to metallic Cu under reaction conditions. The red-Cu/BEA without cofed H_2 exhibited the highest values for r_{C_2}/r_{2MB} and C_{HMB}/C_{HC} ratios, consistent with previous results showing its increased selectivity toward olefins via dehydrogenation. Although red-Cu/BEA + H_2 exhibited a decreased selectivity toward HMB, its deactivation profile was similar to that of H-BEA (Figure S9 in the Supporting Information), suggesting that carbon deposition and/or site blocking is still occurring at a similar rate despite enhanced hydrogenation rates and increased selectivity to hydrocarbons over HMB. Research is ongoing to identify the primary cause of deactivation during the early stages of DME homologation.

Considering the above results, the red-Cu/BEA catalyst possesses both metallic Cu sites and Lewis acidic cationic Cu sites, and both types of sites appear necessary to achieve increases in hydrocarbon productivity, increases in paraffin/olefin ratios, and decreases in selectivity toward aromatics. On the basis of TEM, a large fraction of the metallic Cu nanoparticles were larger than the diameter of the H-BEA pores and thus were located on the external surface of the zeolite. Given the comparison to Cu/SiO_2, the metallic Cu sites activate H_2 at low temperature, decompose some DME into H_2, CO, and CH_4, and hydrogenate ethylene and propylene. Although C_2 and C_3 hydrocarbons accounted for less than 10% of the carbon in the products, the hydrogenation of ethylene and propylene over metallic Cu sites appeared to be directly responsible for both increased hydrocarbon productivity and decreased selectivity toward aromatics, i.e. HMB. We propose that the hydrogenation of ethylene and propylene prevented their entry into the aromatic catalytic cycle via aromatization, and thus caused the observed changes in hydrocarbon productivity and aromatic selectivity.

The cationic Cu sites had low Cu−O coordination numbers and their XAS spectra resembled those for other Cu ion-exchanged zeolites,[17] suggesting that the cationic Cu of the red-Cu/BEA catalyst was ion-exchanged within the pores of the zeolite. These cationic Cu species clearly introduced significant Lewis acidity on the basis of py-DRIFTS, and these sites catalyzed alkane dehydrogenation (i.e., hydrogen recombinative desorption). These findings suggest the formation of cationic Cu−H_x or CuO_x−H species under reaction conditions that can, either independently or in conjunction with a Brønsted acid site, activate C−H bonds, abstract hydrogen, and perform recombinative hydrogen desorption. The dehydrogenation activity of these Cu species suggests that they can facilitate reincorporation of "terminal" alkanes into the chain growth pool during DME homologation via direct dehydrogenation or hydride abstraction and intermolecular hydrogen transfer between an alkane and a surface alkoxide. In the presence of H_2, it is proposed that these cationic Cu species activate H_2 and either hydrogenate olefins or transfer hydrogen to surface alkoxide species to produce alkanes, as evidenced by the increase in C_4−C_7 paraffin/olefin ratios for red-Cu/BEA + H_2. The relative rates of dehydrogenation and hydrogenation/hydrogen transfer over the cationic Cu species as a function of H_2 concentration in the feed is an area of future investigation.

The incorporation of gas-phase D_2 into hydrocarbon products over red-Cu/BEA was observed; however, the exact mechanism for this incorporation is unclear. The incorporation could be explained by one of, or a combination of, the following: (1) a D atom on the metallic Cu or cationic Cu exchanges with the H atom of a hydroxyl on the BEA surface near the perimeter of the Cu particle/ion, followed by subsequent OH−OD exchange on the zeolite surface,[40] (2) olefin hydrogenation with D_2 activated over metallic Cu and/or cationic Cu species, and the formed alkane undergoing hydrogen abstraction and intermolecular hydride transfer to a surface alkoxide within the zeolite, (3) H−D scrambling for DME, methanol, water, and/or alkanes on the metallic Cu surface, followed by desorption and transport into the zeolite, and (4) deuterium spillover from metallic Cu sites to defect sites or carbonaceous species on the BEA zeolite, followed by transport of the D (possibly by a defect generation−annihilation pathway[44]) to a cationic Cu site or other defect site capable of performing hydrogenation/hydrogen transfer. Research to further elucidate the mechanism(s) of H−D exchange and hydrogen incorporation over red-Cu/BEA and its exact role in the catalytic process is ongoing.

4. CONCLUSION

A Cu-modified BEA zeolite, possessing multiple catalytic functionalities (metallic Cu sites, Lewis acidic cationic Cu sites, Brønsted acidity), was demonstrated to incorporate gas-phase H_2 into the desired products, to increase hydrocarbon productivity per site, to increase paraffin selectivity, and to decrease aromatic selectivity while maintaining high selectivity to C_4 and C_7 hydrocarbons. The metallic Cu sites performed H_2 activation and ethylene/propylene hydrogenation, while the cationic Cu sites facilitated hydrogen transfer and hydrogenation of C_4−C_7 olefins produced via the olefin catalytic cycle. These two effects favor the production of hydrocarbons via the olefin pathway over the aromatic pathway.

These findings suggest that H_2 incorporation during DME homologation over a Cu-modified zeolite can achieve high productivity to high-value gasoline-range alkanes, with lower aromatic formation. The combination of metallic and Lewis acidic functionality with Brønsted acid zeolite chemistry presents a pathway toward designing optimized catalysts for homologation reactions in which hydrogen incorporation is desired. Future work will focus on tuning performance by balancing the relative rates of each of the reaction steps.

■ ASSOCIATED CONTENT

Supporting Information

The following file is available free of charge on the ACS Publications website at DOI: 10.1021/cs501876w.

XRD patterns (Figure S1), H_2 TPR profile for Cu-NH_4-BEA (Figure S2), XANES reference spectra (Figure S3), paraffin/olefin molar ratios as a function of TOS (Figure S4), percent difference in C_2−C_3 paraffin/olefin molar ratios in comparison to H-BEA at 6 h TOS (Figure S5),

DOI: 10.1021/cs501876w
ACS Catal. 2015, 5, 1794−1803

mass spectra for propylene and isobutane collected during deuterium incorporation experiments (Figures S6 and S7), ^{2}H NMR spectra for spent catalysts (Figure S8), deactivation profiles (Figure S9), and EXAFS fitting results (Table S1) (PDF)

AUTHOR INFORMATION

Corresponding Author

*E-mail for J.A.S.: Joshua.Schaidle@nrel.gov.

Notes

The authors declare no competing financial interest.

ACKNOWLEDGMENTS

This work was supported by the Laboratory Directed Research and Development Program at the National Renewable Energy Laboratory and the Department of Energy's Bioenergy Technology Office under Contract no. DE-AC36-08-GO28308. X-ray Absorption Spectroscopy was performed at the Advanced Photon Source at Argonne National Laboratory with the assistance of members of the Materials Research Collaborative Access Team (supported by the Department of Energy and the MRCAT member institutions).

REFERENCES

(1) Chang, C. D.; Silvestri, A. J. *J. Catal.* **1977**, *47*, 249−259.
(2) Haw, J. F.; Song, W.; Marcus, D. M.; Nicholas, J. B. *Acc. Chem. Res.* **2003**, *36*, 317−326.
(3) Ilias, S.; Bhan, A. *ACS Catal.* **2012**, *3*, 18−31.
(4) Ahn, J. H.; Temel, B.; Iglesia, E. *Angew. Chem., Int. Ed.* **2009**, *48*, 3814−3816.
(5) Simonetti, D. A.; Ahn, J. H.; Iglesia, E. *J. Catal.* **2011**, *277*, 173−195.
(6) Simonetti, D. A.; Ahn, J. H.; Iglesia, E. *ChemCatChem* **2011**, *3*, 704−718.
(7) Hazari, N.; Iglesia, E.; Labinger, J. A.; Simonetti, D. A. *Acc. Chem. Res.* **2012**, *45*, 653−662.
(8) Kenvin, J. *MicroReport: Micromeritics Instrument Corporation* **2004**, *15*, 8−10.
(9) Emeis, C. A. *J. Catal.* **1993**, *141*, 347−354.
(10) Maier, S. M.; Jentys, A.; Lercher, J. A. *J. Phys. Chem. C* **2011**, *115*, 8005−8013.
(11) Golchoubian, H. *Asian J. Chem.* **2008**, *20*, 5834−5838.
(12) Ressler, T. *J. Synchrotron Radiat.* **1998**, *5*, 118−122.
(13) Newsam, J.; Treacy, M. M.; Koetsier, W.; De Gruyter, C. *Proc. R. Soc. A* **1988**, *420*, 375−405.
(14) Richter, M.; Fait, M. J. G.; Eckelt, R.; Schreier, E.; Schneider, M.; Pohl, M. M.; Fricke, R. *Appl. Catal., B* **2007**, *73*, 269−281.
(15) Szegedi, Á.; Kónya, Z.; Méhn, D.; Solymár, E.; Pál-Borbély, G.; Horváth, Z. E.; Biró, L. P.; Kiricsi, I. *Appl. Catal., A* **2004**, *272*, 257−266.
(16) Kefirov, R.; Penkova, A.; Hadjiivanov, K.; Dzwigaj, S.; Che, M. *Microporous Mesoporous Mater.* **2008**, *116*, 180−187.
(17) Bates, S. A.; Verma, A. A.; Paolucci, C.; Parekh, A. A.; Anggara, T.; Yezerets, A.; Schneider, W. F.; Miller, J. T.; Delgass, W. N.; Ribeiro, F. H. *J. Catal.* **2014**, *312*, 87−97.
(18) Yan, J.; Lei, G.-D.; Sachtler, W.; Kung, H. *J. Catal.* **1996**, *161*, 43−54.
(19) Yan, J. Y.; Sachtler, W. M. H.; Kung, H. H. *Catal. Today* **1997**, *33*, 279−290.
(20) Kieger, S.; Delahay, G.; Coq, B.; Neveu, B. *J. Catal.* **1999**, *183*, 267−280.
(21) Dědeček, J.; Wichterlova, B.; Kubat, P. *Microporous Mesoporous Mater.* **1999**, *32*, 63−74.
(22) Bulánek, R.; Wichterlová, B.; Sobalík, Z.; Tichý, J. *Appl. Catal., B* **2001**, *31*, 13−25.
(23) Kwak, J. H.; Tran, D.; Burton, S. D.; Szanyi, J.; Lee, J. H.; Peden, C. H. F. *J. Catal.* **2012**, *287*, 203−209.
(24) Wang, H.; Xin, W. *Catal. Lett.* **2001**, *76*, 225−229.
(25) Barthel, N.; Finiels, A.; Moreau, C.; Jacquot, R.; Spagnol, M. *J. Mol. Catal. A: Chem.* **2001**, *169*, 163−169.
(26) Salker, A. V.; Weisweiler, W. *Appl. Catal., A* **2000**, *203*, 221−229.
(27) Putluru, S. S. R.; Riisager, A.; Fehrmann, R. *Appl. Catal., B* **2011**, *101*, 183−188.
(28) Hughes, T. R.; White, H. M. *J. Phys. Chem.* **1967**, *71*, 2192−2201.
(29) Amin, N. A. S.; Anggoro, D. D. *J. Nat. Gas Chem.* **2003**, *12*, 123−134.
(30) Zaki, M. I.; Hasan, M. A.; Al-Sagheer, F. A.; Pasupulety, L. *Colloids Surf., A* **2001**, *190*, 261−274.
(31) Parry, E. *J. Catal.* **1963**, *2*, 371−379.
(32) Bezrodna, T.; Puchkovska, G.; Shimanovska, V.; Chashechnikova, I.; Khalyavka, T.; Baran, J. *Appl. Surf. Sci.* **2003**, *214*, 222−231.
(33) Zaki, M. I.; Hasan, M. A.; Pasupulety, L. *Langmuir* **2001**, *17*, 768−774.
(34) Best, R. J.; Russell, W. W. *J. Am. Chem. Soc.* **1954**, *76*, 838−842.
(35) Fisher, I. A.; Bell, A. T. *J. Catal.* **1999**, *184*, 357−376.
(36) Sievers, C.; Onda, A.; Guzman, A.; Otillinger, K. S.; Olindo, R.; Lercher, J. A. *J. Phys. Chem. C* **2006**, *111*, 210−218.
(37) Biscardi, J. A.; Iglesia, E. *Catal. Today* **1996**, *31*, 207−231.
(38) Meitzner, G. D.; Iglesia, E.; Baumgartner, J. E.; Huang, E. S. *J. Catal.* **1993**, *140*, 209−225.
(39) Krishnamurthy, G.; Bhan, A.; Delgass, W. N. *J. Catal.* **2010**, *271*, 370−385.
(40) Prins, R. *Chem. Rev.* **2012**, *112*, 2714−2738.
(41) Sarv, P.; Tuherm, T.; Lippmaa, E.; Keskinen, K.; Root, A. *J. Phys. Chem.* **1995**, *99*, 13763−13768.
(42) Ryder, J. A.; Chakraborty, A. K.; Bell, A. T. *J. Phys. Chem. B* **2000**, *104*, 6998−7011.
(43) Sierka, M.; Sauer, J. *J. Phys. Chem. B* **2001**, *105*, 1603−1613.
(44) Im, J.; Shin, H.; Jang, H.; Kim, H.; Choi, M. *Nat. Commun.* **2014**, *5*, 3370.
(45) Ilias, S.; Bhan, A. *J. Catal.* **2012**, *290*, 186−192.
(46) Ilias, S.; Khare, R.; Malek, A.; Bhan, A. *J. Catal.* **2013**, *303*, 135−140.
(47) Emmett, P.; Skau, N. *J. Am. Chem. Soc.* **1943**, *65*, 1029−1035.
(48) Saadi, A.; Rassoul, Z.; Bettahar, M. *J. Mol. Catal. A: Chem.* **2000**, *164*, 205−216.

DOI: 10.1021/cs501876w
ACS Catal. 2015, 5, 1794−1803